PROCEEDINGS OF SCIENCE

Exotic states (X, Y, Z, Pentaquark et al.)

Marco Pappagallo[*†]
Universitá degli Studi di Bari / INFN Sezione di Bari
E-mail: marco.pappagallo@cern.ch

Leonardo Cristella
Universitá degli Studi di Bari / INFN Sezione di Bari
E-mail: leonardo.cristella@cern.ch

Sandro Palestini
CERN
E-mail: sandro.palestini@cern.ch

The latest results from the ATLAS, CMS and LHCb collaborations in the area of exotic quarkonium decays will be presented. They include: the search for a bottomonium states in the $\Upsilon(1S)\pi^+\pi^-$ mass spectrum, the observation of a peaking structure in the $J/\psi\phi$ mass spectrum from $B^+ \to J/\psi\phi K^+$ decays, a search for the $X(5568)$ state recently claimed by the D0 collaboration and the observation of $J/\psi p$ resonances consistent with pentaquark states in $\Lambda_b \to J/\psi K^- p$ decays.

VII Workshop italiano sulla fisica pp a LHC
16-18 Maggio 2016
Pisa, Italy

[*]Speaker.
[†]On behalf of the LHCb Collaboration.

PoS(PP@LHC2016)010

1. Introduction

The observation of many new states, with masses above the open-charm threshold, that do not fit into the conventional quark model has renewed the interest in *exotic* quarkonium spectroscopy. The X(3872) was discovered by the Belle experiment in 2003 [1] and, despite several detailed studies performed at B-factories, Tevatron and at Large Hadron Collider (LHC), its nature still remains unknown. We report the latest results from the ATLAS, CMS and LHCb collaboration concerning the search for exotic states, such as: the beauty partner of the X(3872) meson, the Y(4140) state observed into the $J/\psi\phi$ decays [7][8], the charged $X(5568)^{\pm}$ state observed into $B_s^0\pi^{\pm}$ [12] and two pentaquarks decaying to $J/\psi p$.

2. Search for the X_b and other hidden-beauty states

Heavy-quark symmetry suggests the existence of a hidden-beauty partner of the X(3872) referred to as X_b, which should be produced in pp collisions.

2.1 ATLAS

ATLAS experiment has performed a search for this particle in $\pi^+\pi^-\Upsilon(1S)$ channel with the pp collision data collected at $\sqrt{s} = 8$ TeV in 2012. The $\Upsilon(1S)$ candidates are built from two muon tracks. The candidates with the invariant mass within ± 350 MeV window around the nominal $\Upsilon(1S)$ mass are retained. They are combined with two tracks assigned pion mass hypotheses and a 4-prong vertex fit is performed. The muon pair mass is constrained to the world average for the $\Upsilon(1S)$ to improve the $X_b \to \pi^+\pi^-\Upsilon(1S)$ mass resolution.

The whole data sample is separated into 8 kinematic bins with different signal sensitivity. First, based on the rapidity y of the X_b candidate, the barrel ($|y| < 1.2$) and endcap ($1.2 < |y| < 2.4$) regions having different invariant mass resolution are separated. Each of these sub-samples is then split into four bins with different signal-to-background ratio. This splitting is defined using the candidate transverse momentum p_{T} and $\cos\theta^*$, where θ^* is an angle between $\pi^+\pi^-$ combined momentum in the parent momentum rest frame and the parent momentum in the laboratory frame. Expected fractions of the signal in each bin are defined by splitting functions derived from the simulation.

Figure 1 shows the distribution of the $\pi^+\pi^-\Upsilon(1S)$ invariant mass. Only peaks at the masses corresponding to $\Upsilon(2S)$ and $\Upsilon(3S)$ signals are seen. These signals are used to validate correctness of the splitting functions and check agreement of the yields between data and simulation.

To search for the X_b signal, a hypothesis test for the presence of a peak is performed every 10 MeV in the $\pi^+\pi^-\Upsilon(1S)$ mass range from 10 GeV to 11 GeV. At each mass, a simultaneous fit to all analysis bins is performed. A double Gaussian function is used in the fits for the expected signal shape thus assuming its width to be negligible with respect to the detector resolution. Other constraints used in the fit procedure assume the resolution dependence on y and p_{T} being the same as that for $\Upsilon(2,3S)$ states and the phase-space distribution of the di-pion invariant mass.

An upper limit on the value of $R = (\sigma\cdot\mathscr{B})/(\sigma\cdot\mathscr{B})_{2S}$ is set using the CL_S method by implementing asymptotic formulae for the $\tilde{q}_\mu$ statistic [5]. The $(\sigma\cdot\mathscr{B})$ is a product of the hypothetical state production cross-section and the branching fraction of its decay to $\pi^+\pi^-\Upsilon(1S)$ while

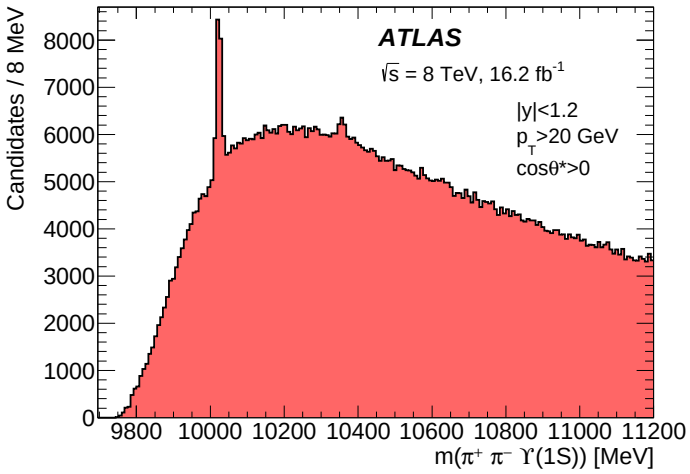

Figure 1: The $\pi^+\pi^-\Upsilon(1S)$ invariant mass distribution in the kinematic bin most sensitive to an X_b signal. The only apparent peaks are at the masses of the $\Upsilon(2S)$ (10023 MeV) and $\Upsilon(3S)$ (10355 MeV). Figure taken from Ref. [4].

$(\sigma\cdot\mathscr{B})_{2S}$ is the same quantity for the $\Upsilon(2S)$. Various systematic uncertainties were studied and included in the fit likelihood as nuisance parameters to be accounted in the limit setting. Figure 2 shows the 95% CL_S limit on R as a function of the X_b mass. The mass regions close to $\Upsilon(2S)$ and $\Upsilon(3S)$ resonances are excluded from the analysis due to poor sensitivity.

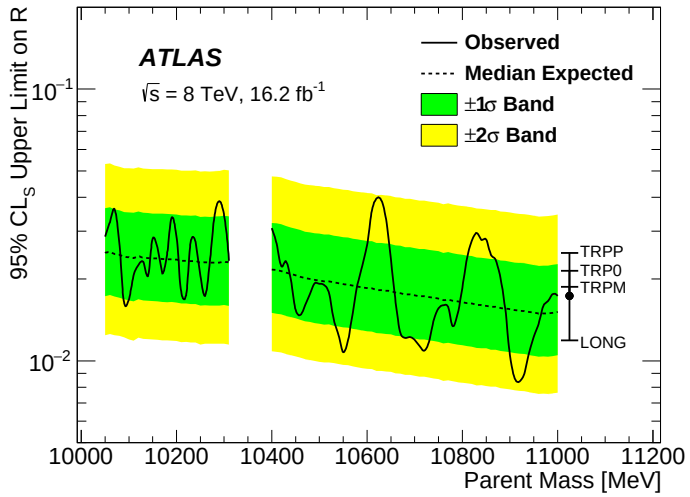

Figure 2: Observed 95% CL_S upper limits (solid line) on the relative production rate $R = (\sigma\cdot\mathscr{B})/(\sigma\cdot\mathscr{B})_{2S}$ of a hypothetical X_b parent state decaying isotropically to $\pi^+\pi^-\Upsilon(1S)$, as a function of mass. The median expectation (dashed) and the corresponding $\pm1\sigma$ and $\pm2\sigma$ bands (green and yellow respectively) are also shown. The bar on the right shows typical shifts under alternative X_b spin-alignment scenarios, relative to the isotropic ("FLAT") case shown with the solid point. Figure taken from Ref. [4].

The procedure assumes unpolarised production of the X_b state. However the X_b spin-alignment is unknown and can have a strong impact on the upper limit calculation. Rather than including this as a systematic uncertainty, upper limits are recalculated under longitudinal ("LONG") and

three transverse ("TRPP", "TRP0", "TRPM") spin-alignment scenarios. Shifts in the upper limits (either up or down) depend only weakly on mass. Thus in Figure 2 the effect of each hypothesis is represented by a single number, chosen as a difference in the median expected CL_S from the unpolarised ('FLAT') case.

No evidence of X_b signal is found. An 95% CL_S upper limit on $(\sigma \cdot \mathscr{B})/(\sigma \cdot \mathscr{B})_{2S}$ is set at level of 0.8–4.0% depending on mass. The analogous ratio for the $X(3872)$ state is 6.56%: a value this large is excluded for all X_b masses considered.

Within the same analysis framework, searches for the $\Upsilon(1^3D_J)$ triplet as well as for wide resonances $\Upsilon(10860)$ and $\Upsilon(11020)$ states were performed. For these signals, the fit model was modified accordingly. None of these searches resulted in a signal evidence. For the triplet, an upper limit on the ratio of cross-sections $\sigma(\Upsilon(1^3D_J))/\sigma(\Upsilon(2S)) < 0.55$ was set.

2.2 CMS

CMS looked for the X_b state [6] in events with a $\Upsilon(1S)$ candidate and two additional opposite-charged tracks, assumed to be pions. A common vertex has been fitted with muons and pions, and the invariant mass has been computed by constraining the dimuon mass to the $\Upsilon(1S)$. The mass distribution are shown in Figure 3, for rapidity intervals in the barrel and endcap regions, where the two peaks corresponding to $\Upsilon(2S)$ and $\Upsilon(3S)$ are visible.

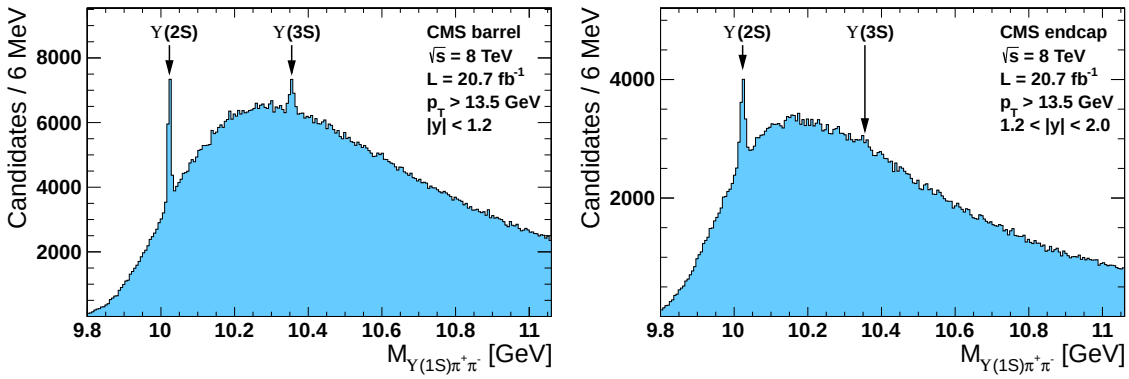

Figure 3: Reconstructed invariant-mass distributions of the candidate in the barrel (left) and endcap (right) regions.

The ratio R of cross-sections for X_b and $\Upsilon(2S)$ was estimated for different hypotheses about X_b mass. The search has been performed in two regions, [10.05, 10.31] GeV and [10.40, 10.99] GeV, to exclude the $\Upsilon(2S)$ and $\Upsilon(3S)$; the mass spectrum has been fitted with a gaussian function for the resonances and a polynomial for the background. The X_b mass has been shifted by 10 MeV steps, while its width has been assumed to be small, and the resolution was taken from simulation. The ratio R was then given by the ratio of the observed candidates scaled with the ratio of efficiencies. Signal strength, P-values and cross section limits have been computed versus X_b mass. Results are shown in Figure 4.

Systematic uncertainties have been estimated by considering different models for dipion mass distribution and varying the efficiency dependence on X_b mass. Different models for the mass

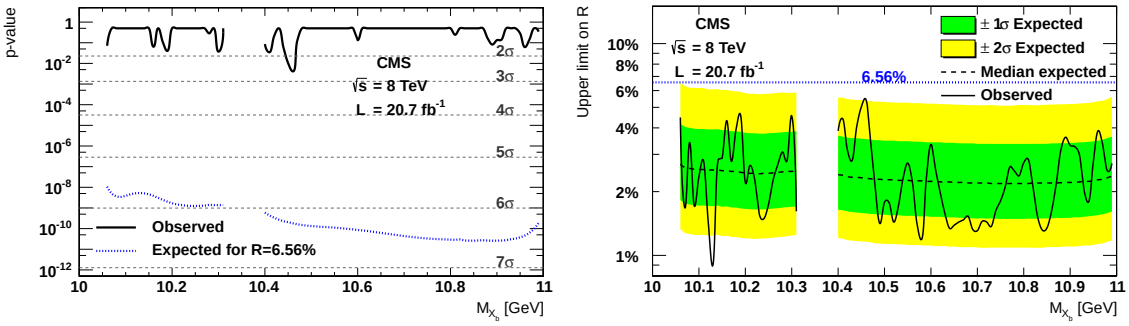

Figure 4: P-value (left) and upper limit at 95% confidence level on R (right) as a function of the assumed X_b mass. The lines at 6.56% correspond to the expectations for the analogous $X(3872)$ decay to $J/\psi\pi^+\pi^-$.

distributions and resolutions have been considered as well as different assumptions for the X_b polarization.

3. Y(4140)

The CDF collaboration observed the $Y(4140)$ structure with a significance greater than 5σ [7][8], while LHCb collaboration did not confirm it and put an upper limit to its production [9]. All the details of this study, exploiting the data recorded by CMS in 2011 (corresponding to an integrated luminosity of $5.2\,fb^{-1}$), are reported in [10]. The selection criteria, designed to maximize the B signal yield, were determined before examining the mass difference $\Delta m \equiv m(\mu^+\mu^-K^+K^-) - m(\mu^+\mu^-)$, that is the observable used to search for possibile structures in the $J/\psi\phi$ mass. After performing a background subtraction and correcting for relative efficiency the resulting Δm distribution and its 1D-fit is shown in Fig. 5 (right): two peaking structures are observed above the phase-space (PS) continuum distribution. On the plot is also shown the result of a 2D simultaneous fit of both B^+ invariant mass and Δm distributions with implicit background subtraction and efficiency correction.

Interpreting the two structures as $J/\psi\phi$ resonances with S-wave relativistic Breit-Wigner lineshapes laying over a residual three-body phase-space non-resonant component, the fitted mass of the structure close to the kinematical threshold is $m = (4148.2 \pm 2.0(stat.) \pm 4.6(sys.))$ MeV; this structure is observed with a significance exceeding 5σ and is consistent with a previous evidence by the CDF Collaboration [7].

The $J/\psi\phi$ system should be properly studied with more data by performing an amplitude analysis of this five-body decay able to properly account for eventual ϕK^+ resonances.

4. Search for structure in the $B_s^0\pi^\pm$ invariant mass spectrum

In february the D0 collaboration has claimed [12] the observation with $5.1\,\sigma$ significance of a narrow structure, which they dub the $X(5568)$, in the decay sequence $X(5568) \to B_s^0\pi^\pm$, $B_s^0 \to J/\psi\phi$, $J/\psi \to \mu^+\mu^-$, $\phi \to K^+K^-$. The mass and width of the $X(5568)$ state are reported to be $m = 5567.8 \pm 2.9^{+0.9}_{-1.9}\,\mathrm{MeV/c^2}$ and $\Gamma = 21.9 \pm 6.4^{+5.0}_{-2.5}\,\mathrm{MeV/c^2}$. The fraction of B_s^0 mesons

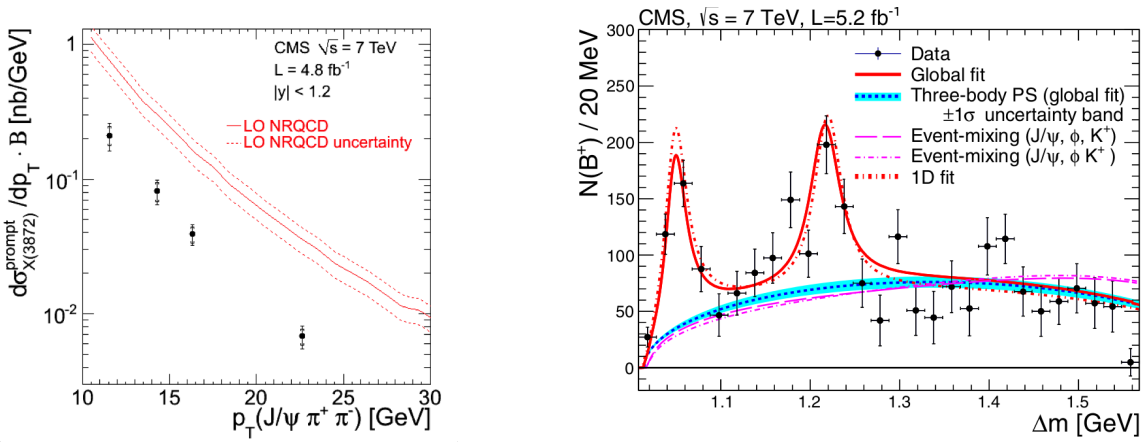

Figure 5: Left: measured differential cross section for prompt $X(3872)$ production times branching fraction of $X(3872) \to J/\psi\pi^+\pi^-$ as a function of p_T. The inner error bars indicate the statistical uncertainty while the outer error bars represent the total uncertainty. Prediction from [11] are shown by the lines and data points are placed where the theoretical value is equal to its mean value over each bin. Right: number of $B^+ \to J/\psi\phi K^+$ candidates as a function of $\Delta m = m(\mu^+\mu^- K^+ K^-) - m(\mu^+\mu^-)$. The solid curve is the global UML fit of the data, and the dotted curve is the background contribution assuming three-body PS. The band is the $\pm 1\sigma$ uncertainty range for the background obtained from the global fit. The dashed and dash-dotted curves are background curves obtained from two different event-mixing procedures and normalized to the number of three-body PS background events. The short dashed curve is the 1D fit to the data.

that comes from $X(5568) \to B_s^0\pi^\pm$ decay is reported to be $\rho_X^{\mathrm{D0}} = (8.6 \pm 1.9 \pm 1.4)\,\%$. Recently the significance of the signal has been revisited after loosening the selection of the $B_s^0\pi^\pm$ candidates.

The claimed $X(5568)$ state has been searched in a data sample corresponding to $3fb^{-1}$ of pp collision data at $\sqrt{s} = 7$ and 8 TeV recorded by LHCb [13]. The B_s^0 mesons are reconstructed in decays to $D_s^-\pi^+$ and $J/\psi\phi$ final states to obtain a B_s^0 yield approximately 20 times larger than that available to the D0 collaboration. The analysis techniques follow closely those developed for studies of the B^+K^- [14], $B^+\pi^-$ and $B^0\pi^+$ [15] spectra. The B_s^0 candidates are combined with each track that originates from the same primary vertex and that has $p_T > 500$ MeV/c.

The $Q \equiv m(B_s^0\pi) - M_{B_s^0} - M_\pi$ distributions are fitted with a function containing components for signal and background. The signal shape is an S-wave Breit–Wigner function, with mass and width parameters fixed according to the central values obtained by the D0 collaboration. The resolution is less than 1 MeV/c^2 in the Q value region of interest, and is neglected. The background is modelled with a polynomial function. The two B_s^0 decay modes are fitted simultaneously. The fit has a p-value of 34.0% and no significant $X(5568)$ yield. Results of fits where the signal yield is fixed to zero are shown in Fig. 6(a).

The results of the fits to the $B_s^0\pi^\pm$ Q value distributions are used to measure the ratio of cross-sections

$$\rho_X^{\mathrm{LHCb}} \equiv \frac{\sigma(pp \to X(5568) + \text{anything}) \times \mathscr{B}\left(X(5568) \to B_s^0\pi^\pm\right)}{\sigma(pp \to B_s^0 + \text{anything})}, \tag{4.1}$$

$$= \frac{N(X)}{N(B_s^0)} \times \frac{1}{\varepsilon^{\mathrm{rel}}(X)}, \tag{4.2}$$

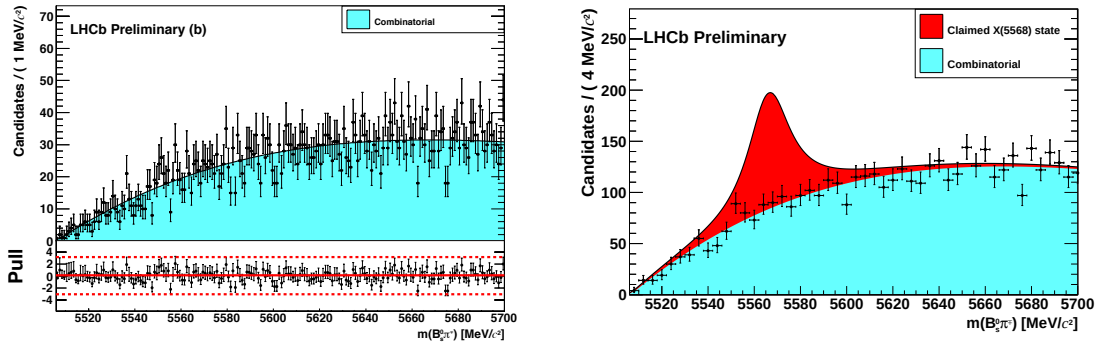

Figure 6: (left) Results of the fit to the Q value distribution, shifted to display the $B_s^0\pi^+$ invariant mass, for $B_s^0\pi$ candidates (both B_s^0 modes combined) with the signal yield fixed to zero. The fits are shown for minimum B_s^0 p_T of 10 GeV/c^2. (right) Distribution of Q value, shifted to display the $B_s^0\pi^+$ invariant mass (both B_s^0 modes combined), for candidates with minimum B_s^0 p_T of 10GeV/c^2, with a signal component superimposed that corresponds to $\rho_X^{\rm LHCb} = 8.6\,\%$.

where the cross-sections σ are for promptly produced particles within the LHCb acceptance. The relative efficiency $\varepsilon^{\rm rel}(X) = \frac{\varepsilon(X)}{\varepsilon(B_s^0)}$ is determined from simulation and accounts for the reconstruction and selection efficiency of the companion pion as well as the requirement that is within the LHCb acceptance. Many systematic uncertainties are considered and the dominant sources are due to the variation of the signal width and the effect of the efficiency on the signal shape.

Since the signal is not significant, upper limits on $\rho_X^{\rm LHCb}$ are obtained by integration of the likelihood in the positive region to find the value that contains the fraction of the integral corresponding to the required confidence level (CL). The upper limits are found to be

$$\rho_X^{\rm LHCb}(B_s^0\ p_T > \ \ 5\ {\rm GeV/c^2}) < 0.009\,(0.010)\ @\ 90\,(95)\,\%\ {\rm CL},$$
$$\rho_X^{\rm LHCb}(B_s^0\ p_T > 10\ {\rm GeV/c^2}) < 0.016\,(0.018)\ @\ 90\,(95)\,\%\ {\rm CL}.$$

5. Observation of $J/\psi p$ resonances consistent with pentaquark states in $\Lambda_b \to J/\psi K^- p$ decays

Past claimed observations of pentaquark states have been shown to be spurious but the existence of pentaquark baryon states would not be surprising given the observation of charged charmonium-like meson (e.g. $Z_c(4430)^+$). A large sample (26,000 candidates) of Λ_b baryons decaying to the $J/\psi K^- p$ final state has been reconstructed at LHCb (Fig. 7(a)) [17]. In Fig. 7(b) the Dalitz plot is shown using the Kp and J/ψ invariant masses-squared as independent variables. A distinct vertical band is observed in the Kp invariant mass distribution near 2.3 GeV/c^2 corresponding to the $\Lambda(1520)$ resonance. There is also a distinct horizontal band near 19.5 GeV/c^2. In order to ascertain if the observed structures are resonant in nature and not due to reflections generated by the Λ^* states, it is necessary to perform a full amplitude analysis, allowing for interference effects between both decay sequences.

The fit uses five decay angles and the $K^- p$ invariant mass m_{Kp} as independent variables. First the data were fit with an amplitude model that contains 14 Λ^* states listed by the Particle Data

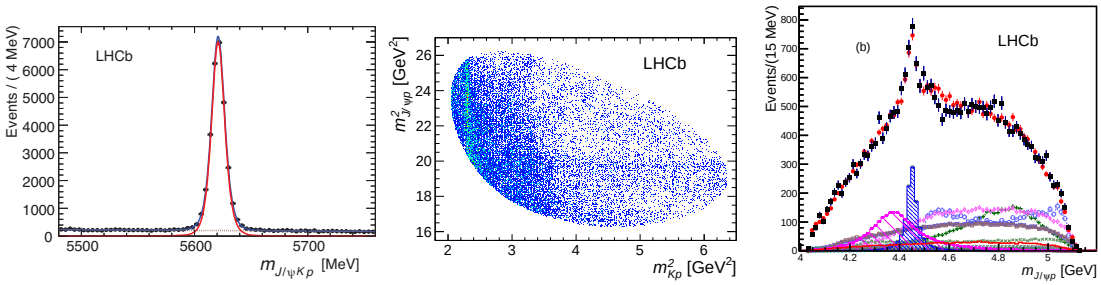

Figure 7: (left) Invariant mass spectrum of $J/\psi K^- p$ combinations, with the total fit, signal and background components shown as solid (blue), solid (red) and dashed lines, respectively. (Middle) Invariant mass squared of $K^- p$ versus $J/\psi p$ for candidates within ± 15 MeV of the Λ_b mass. (right) Fit projections for $m_{J/\psi p}$ for the reduced Λ^* model with two P_c^+ states. The data are shown as solid (black) squares, while the solid (red) points show the results of the fit. The solid (red) histogram shows the background distribution. The (blue) open squares with the shaded histogram represent the $P_c(4450)^+$ state, and the shaded histogram topped with (purple) filled squares represents the $P_c(4380)^+$ state. Each Λ^* component is also shown. The error bars on the points showing the fit results are due to simulation statistics.

Group. As this did not give a satisfactory description of the data, one P_c^+ state was added, and when that was not sufficient a second state was included. The two P_c^+ states are found to have masses of $4380 \pm 8 \pm 29$ MeV and $4449.8 \pm 1.7 \pm 2.5$ MeV, with corresponding widths of $205 \pm 18 \pm 86$ MeV and $39 \pm 5 \pm 19$ MeV. The best fit solution has spin-parity J^P values of $(3/2^-, 5/2^+)$. Acceptable solutions are also found for additional cases with opposite parity, either $(3/2^+, 5/2^-)$ or $(5/2^+, 3/2^-)$. The best fit projections are shown in Fig. 7(c). The significances of the lower mass and higher mass states are 9 and 12 standard deviations, respectively.

Further evidence for the resonant character of the higher mass, narrower, P_c^+ state is obtained by viewing the evolution of the complex amplitude in the Argand diagram [18]. In the amplitude fits discussed above, the $P_c(4450)^+$ is represented by a Breit-Wigner amplitude, where the magnitude and phase vary with $m_{J/\psi p}$ according to an approximately circular trajectory in the $(\mathrm{Re}A^{P_c}, \mathrm{Im}A^{P_c})$ plane, where A^{P_c} is the $m_{J/\psi p}$ dependent part of the $P_c(4450)^+$ amplitude. An additional fit to the data has been performed, in which the $P_c(4450)^+$ amplitude is represented as the combination of independent complex amplitudes at six equidistant points in the range $\pm\Gamma_0 = 39\,\mathrm{MeV}$ around $M_0 = 4449.8\,\mathrm{MeV}$ as determined in the default fit. Real and imaginary parts of the amplitude are interpolated in mass between the fitted points. The resulting Argand diagram, shown in Fig. 8(a), is consistent with a rapid counter-clockwise change of the $P_c(4450)^+$ phase when its magnitude reaches the maximum, a behavior characteristic of a resonance. A similar study for the wider state is shown in Fig. 8(b); although the fit does show a large phase change, the amplitude values are sensitive to the details of the Λ^* model and so this latter study is not conclusive.

In order to investigate further the presence of pentaquarks in the $\Lambda_b \to J/\psi p K^-$ decay chain, a model-independent analysis has been carried out [16]. It has been demonstrated at more than 9 standard deviations that the $\Lambda_b \to J/\psi p K^-$ decays cannot all be attributed to $K^- p$ resonant or nonresonant contributions. The analysis requires only minimal assumptions on the mass and spin of the $K^- p$ contributions; no assumptions on their number, their resonant or nonresonant nature, or their lineshapes have been made. Non-$K^- p$ contributions, which must be present in the data, can be

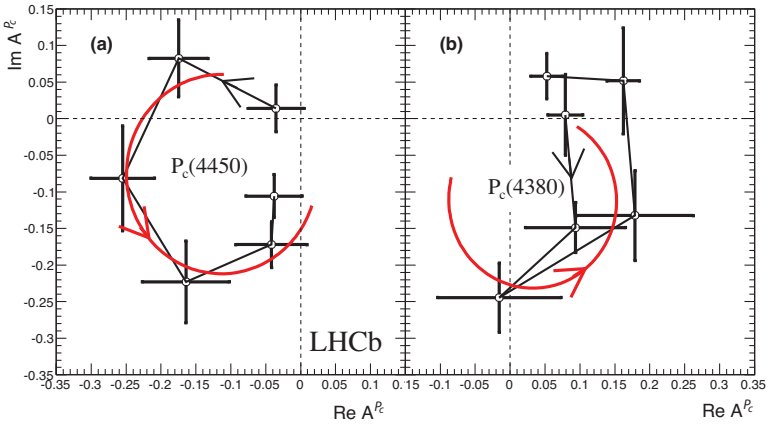

Figure 8: Fitted values of the real and imaginary parts of the amplitudes for the baseline $(3/2^-, 5/2^+)$ fit for a) the $P_c(4450)^+$ state and b) the $P_c(4380)^+$ state, each divided into six $m_{J/\psi p}$ bins of equal width between $-\Gamma_0$ and $+\Gamma_0$ shown in the Argand diagrams as connected points with error bars ($m_{J/\psi p}$ increases counterclockwise). The solid (red) curves are the predictions from the Breit-Wigner formula for the same mass ranges with M_0 (Γ_0) of 4450 (39) MeV and 4380 (205) MeV, respectively, with the phases and magnitudes at the resonance masses set to the average values between the two points around M_0. Systematic uncertainties are not included.

either of the exotic hadron type, or due to rescattering effects among ordinary hadrons. This result supports the amplitude model-dependent observation of the $J/\psi p$ resonances presented previously [17].

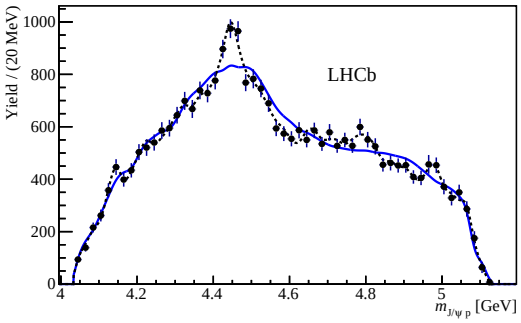

Figure 9: Efficiency-corrected and background-subtracted $m_{J/\psi p}$ distribution of the data (black points with error bars), with $PDF(m_{J/\psi p}|H_0)$ (solid blue line) and $PDF(m_{J/\psi p}|H_1)$ (dashed black line) superimposed.

6. Summary

The search for a bottomonium states in the $\Upsilon(1S)\pi^+\pi^-$ mass spectrum in both CMS and ATLAS shows no evidence of an X_b signal. An upper limit on the value of $R = (\sigma \cdot \mathscr{B})/(\sigma \cdot \mathscr{B})_{2S}$ is set from both experiments using the CL_S method.

The CMS observation of the first structure in the $J/\psi\phi$ mass spectrum in B hadron decays is consistent with a previous evidence by the CDF Collaboration. The analyzed 2011 data do not,

however, provide a sufficiently large and pure sample for this purpose. The $J/\psi\phi$ system should be properly studied by performing an amplitude analysis of this five-body decay able to take into account the helicity configurations of the decay products.

No signal of $X(5568)^{\pm}$ has been observed in the LHCb rapidity range while a model independent analysis of the $\Lambda_b \to J/\psi p K^-$ decays supports the existence of the two pentaquarks observed previously by an amplitude analysis.

References

[1] S.K. Choi *et al.* [Belle Collaboration], Phys. Rev. Lett. **91** (2003) 262001.

[2] K. Abe *et al.* [Belle Collaboration], Phys. Rev. Lett. **94** (2005) 182002.

[3] B. Aubert *et al.* [Babar Collaboration], Phys. Rev. Lett. **101** (2008) 082001.

[4] G. Aad *et al.* [ATLAS Collaboration], Phys. Lett. B **740** (2015) 199.

[5] G. Cowan, K. Cranmer, E. Gross and O. Vitells, Eur. Phys. J. C **71** (2011) 1554.

[6] S. Chatrchyan *et al.* [CMS Collaboration], Phys. Lett. B **727** (2013) 57.

[7] T. Aaltonen *et al.* [CDF Collaboration], Phys. Rev. Lett. **102** (2009) 242002.

[8] T. Aaltonen *et al.* [CDF Collaboration], arXiv:1101.6058.

[9] R. Aaij *et al.* [LHCb Collaboration], Phys. Rev. D **85** (2012) 091103.

[10] S. Chatrchyan *et al.* [CMS Collaboration], Phys. Lett. B **734** (2014) 261.

[11] P. Artoisenet and E. Braaten, Phys. Rev. D **81** (2010) 114018.

[12] V. M. Abazov *et al.* [D0 Collaboration], Phys. Rev. Lett. **117** (2016), 022003.

[13] R. Aaij *et al.* [LHCb Collaboration], LHCb-CONF-2016-004.

[14] R. Aaij *et al.* [LHCb Collaboration], Phys. Rev. Lett. **110** (2013) 151803.

[15] R. Aaij *et al.* [LHCb Collaboration], JHEP **1504** (2015) 024.

[16] R. Aaij *et al.* [LHCb Collaboration], Phys. Rev. Lett. **117** (2016) 082002.

[17] R. Aaij *et al.* [LHCb Collaboration], Phys. Rev. Lett. **115** (2015) 072001.

[18] K. A. Olive *et al.* (Particle Data Group), Chin. Phys. C, 38, 090001 (2014).